Multiobjective Optimization of Post-Tensioned Concrete Box-Girder Road Bridges Considering Cost, CO_2 emissions, and Safety

Tatiana García-Segura[1]

Víctor Yepes[2]

Abstract

This paper presents a multiobjective optimization of post-tensioned concrete road bridges in terms of cost, CO_2 emissions, and overall safety factor. A computer tool links the optimization modulus with a set of modules for the finite-element analysis and limit states verification. This is applied for the case study of a three-span continuous post-tensioned box-girder road bridge, located in a coastal region. A multiobjective harmony search is used to automatically search a set of optimum structural solutions regarding the geometry, concrete strength, reinforcing and post-tensioned steel. Diversification strategies are combined with intensification strategies to improve solution quality. Results indicate that cost and CO_2 emissions are close to each other for any safety range. A one-euro reduction, involves a 2.34 kg CO_2 emissions reduction. Output identifies the best variables to improve safety and the critical limit states. This tool also provides bridge managers with a set of trade-off optimum solutions, which balance their preferences most closely, and meet the requirements previously defined.

Keywords

Multiobjective optimization; CO_2 emissions; safety; post-tensioned concrete; box-girder bridge; multiobjective harmony search

[1] Graduate Research Assistant, Institute of Concrete Science and Technology (ICITECH), *Universitat Politècnica de València*, 46022 Valencia, Spain. E-mail: tagarse@cam.upv.es

[2] Associate Professor, Institute of Concrete Science and Technology (ICITECH), *Universitat Politècnica de València*, 46022 Valencia, Spain. **Corresponding author**. Phone +34963879563; Fax: +34963877569; E-mail: vyepesp@cst.upv.es

1. Introduction

Traditional methods for bridge design involve a trial-and-error procedure. The geometrical layout is *a priori* defined to perform the structural analysis. The stresses and displacement are compared with the allowable values, according to the code specifications. The dimensions are modified if the limits are not satisfied, otherwise, the remaining variables of the reinforcing steel are calculated based on the code's ultimate limit states. The final design does not guarantee to be optimal. That is the structural optimization has attracted the interest of many researchers.

Bridge optimization captured engineers' attention from the 1970s onwards, including reinforcing slab bridges [1], precast-prestressed concrete girders [2–4], steel girders [5], and cast-in-place prestressed concrete box girders [6,7]. Exact methods based on sequential techniques of mathematical programming evolved towards heuristic optimization. A review of heuristic algorithms applied to structural optimization is presented in the study of Hare et al. [8]. These algorithms appear to be a reliable approach for complex and realistic structural optimization problems. Constraints on structural design code can be incorporated in a straightforward manner, in contrast to mathematical programming optimizers, which require the calculation of gradients of the constraints [9].

Srinivas and Ramanjaneyulu [10] minimized the cost of a T-girder bridge deck system using artificial neural networks and genetic algorithms. Perea et al. [11] implemented several heuristic search methods to effectively design reinforced-concrete bridge frames. Martinez et al. [12] proposed a variant of ant-colony optimization to optimize tall bridge piers. Rana et al. [13] presented an evolutionary operation, based on a global optimization algorithm for the minimum cost design of a two-span, continuous, prestressed concrete (PC) I-girder bridge structure. A hybrid simulated annealing algorithm [14] and a memetic algorithm with variable-depth neighborhood search [15] were applied to find the most economical solution for precast-prestressed concrete U-beam road bridges. After studying the robustness of ant colonies, genetic algorithms, harmony search (HS), simulated annealing, particle swarm optimization and tabu search (TS), Alberdi et al. [16] indicated that the most robust algorithms were HS and TS. Findings also indicated the benefits of combining intensification and diversification techniques.

While these approaches have been advocated for optimal bridge design in terms of cost, other objectives have been the focus of research, with aspects regarding structural sustainability gaining increased attention. CO_2 emissions were incorporated as an environmental objective to be compared with economic designs of reinforced concrete (RC) frames [17,18], RC retaining walls [19], RC footings [20] precast-prestressed concrete U-beam road bridges [21] and post-tensioned concrete box-girder pedestrian bridges [22]. Although CO_2 emissions are a common indicator, other environmental impact assessment indicators can be used to achieve an environmentally friendly structure [23]. Some studies detected that optimal solutions in terms of monetary costs have satisfactory environmental outcomes [21–23], while others found cost increments when CO_2 emissions decreased [20,24]. The environmental and economic costs of materials are not proportional. Therefore, the grade to which each criterion moves away from the structural efficiency, and the range of choices of the structure within the feasible space, determine the relationship between the optimization objectives. The former paper written by the authors [22] studied the optimum solutions of pedestrian bridges by a monobjective optimization of the cost and CO_2 emissions. This paper focuses on the multiobjective optimization of post-tensioned concrete road bridges regarding cost, CO_2 emissions, and overall safety factor. The overall safety factor is considered as an objective function to analyze the degree of dependence between the space of feasible solutions and the relationship cost-CO_2 emissions. In addition, the optimum value of the variables is investigated according to the level of safety requirements.

Many real-world engineering designs are characterized by the presence of conflicting objectives. In this case, the problem should be formulated as a multiobjective optimization problem. Zavala et al. [25] presented a survey of multiobjective metaheuristics applied to structural optimization. Lifetime condition, safety levels and life-cycle maintenance cost were computed as objectives for the multiobjective optimization problem of deteriorating bridges [26]. Constructability, economic cost, environmental impact, and overall safety were chosen to efficiently design RC building frames [27]. Quaglia et al. [28] studied the trade-off between the structural performance and energy efficiency of a deployable shelter. The study of Yepes et al. [29] proposed costs, CO_2 emissions, and service life as criteria for attaining a sustainable structural design. Converting the structural safety constraints to objectives allows finding multiple trade-off solutions that hardly increase the cost and achieve improved safety. This is important when the structure is expected to be under increased loads, or the deterioration process may cause a reduction in structural safety.

In this paper, the sustainability of post-tensioned concrete box-girder road bridges is quantified in terms of economic cost, CO_2 emissions including carbonation, and the overall safety factor. These criteria seek a balance among the cost associated with construction materials and placement, the embedded emissions resulting from material production, transport and CO_2 capture, and the benefits achieved through improving structural safety prior to failure. To seek the set of optimum solutions, a modified multiobjective harmony search is proposed, using techniques of diversification and intensification. The algorithm, based on searching the perfect harmony, uses this strategy to systematically choose the discrete values of geometry, concrete strength, reinforcement and post-tensioned steel. In order to conduct a precise analysis of a real post-tensioned concrete bridge, a computer tool is developed to connect a finite-element software with the optimization procedure. This paper provides a methodology for the automatic design of bridges through a commercial software for finite element analysis. The aim of this study is to: (1) provide an automatic design process for bridges with multiple objectives; (2) analyze the relationship between the criteria; (3) check if the relationship between cost and CO_2 changes according to the safety requirements; (4) provide multiple trade-offs and high-performing solutions; and (5) discover useful knowledge regarding the best variables to improve safety.

2. Definition of multiobjective optimization problem

A multiobjective harmony search was used to optimize the geometrical design, concrete strength, reinforcement and post-tensioned steel of box-girder road bridges. The vector x contains the design variables, which are discrete to guarantee a real bridge design. The objective functions considered are the economic cost (C), CO_2 emissions (E), and the overall safety factor (S). The multiobjective optimization minimizes the cost (Eq. (1)) and the emissions (Eq. (2)), while maximizing the overall safety factor (Eq. (3)). The Pareto front is defined by the set of non-dominated solutions. These solutions cannot be improved without worsening the value of one objective. The constraints (Eq. (4)) represent all the serviceability limit states (SLSs) and the ultimate limit states (ULSs), as well as the geometric and constructability constraints that the structure must satisfy.

$$\min \mathrm{C}(\vec{x}) \tag{1}$$

$$\min \mathrm{E}(\vec{x}) \tag{2}$$

$$\max \mathrm{S}(\vec{x}) \tag{3}$$

$$G_j(\vec{x}) \leq 0 \tag{4}$$

2.1. Design variables and parameters

The structural problem involves a three-span continuous post-tensioned concrete (PSC) box-girder road bridge located in a coastal region. The main span has a length (L_1) of 44 m and a width of 11.8 m. The highway has two 3.5 m-wide lanes, a 1m-wide inner verge and a 2.5 m-wide outer verge. Moreover, 65 cm space is provided on both sides to place the parapet. The external spans (L_2) have a ratio of 0.8 between the main span. The construction is considered to be cast in place. The scaffolding is not considered, since it does not entail any change with respect to the optimal solution. The bridge is located in a coastal environment.

Fig. 1 shows the variables. The cross-section geometry is defined by eight variables: the depth (h), the width of the bottom slab (b), the width of the web inclination (d), the thickness of the top slab (e_s), the thickness of the external flange section (e_v), the thickness of the internal flange section (e_{va}), the thickness of the bottom slab (e_i) and the thickness of the webs (e_a). The width of the web inclination is determined from the web slope. The range of possible values for the web slope is between 2 and 4. The haunch lengths (t_1, t_2, t_3, t_4) are not variables, since they are determined by the value of other variables (Eq. (5–8)).

$$t_1 = e_{va} - e_s \tag{5}$$

$$t_2 = \frac{b+2*d}{5} \tag{6}$$

$$t_3 = e_i \tag{7}$$

$$t_4 = \frac{b}{10} \tag{8}$$

One variable defines the concrete strength (f_{ck}), ranging from 35 MPa to 100 MPa. The concrete is post-tensioned with strands distributed symmetrically through the webs by a parabolic layout (see Fig. 2). The variables are the eccentricity in the external spans (e_p) as a ratio of half of the bridge depth, the distance

from the piers to the point of inflection (L_{pi}) as a ratio of the span length, and the number of strands (N_S). The eccentricity in the external spans where the bending moment is maximum has a distance of $0.375 \cdot L_2$ from the abutments. The eccentricity in the supports and midspan of the central span is the maximum allowed. The distance between the center of the duct and the reinforcing bars must be 1.5 times that of the duct diameter. A further consideration is that of the space for the duct placement. Over piers, the ducts are allocated in the flanges and top slab. The lower points of layout are placed in rows of two. Each strand is prestressed to 195.52 KN.

The diameter of the longitudinal reinforcing steel is defined by 10 variables (LR_1, LR_2, LR_3, LR_4, LR_5, LR_6, LR_7, LR_8, LR_9, LR_{10}). The extra reinforcement in the top slab (LR_7, LR_8) and in the bottom slab (LR_9, LR_{10}) covers the pier zone (L/5 on both sides of the piers) and the rest of the span, respectively. The feasible set for the diameter variable includes 10, 12, 16, 20, 25 and 32 mm. However, the extra reinforcement can also adopt the value 0. Nine variables determine the diameter of the transverse reinforcement (TR_1, TR_2, TR_3, TR_4, $TR_{4'}$, TR_5, TR_6, TR_7, TR_8). The extra reinforcement in $TR_{4'}$ is placed at the same position as TR_4 and covers the support zone. To improve the efficiency over the flanges, the extra reinforcement TR_8 covers this length. TR_9 is fixed as 12mm. Finally, for the sake of the construction simplicity, the number of bars per meter for all the longitudinal reinforcing is equal. The number of bars per meter (N_{LR}) can take the values: 4, 5 and 6. Likewise, the spacing of all the transverse reinforcing (S_{TR}) is equal. The values can be 15, 20 and 25 cm.

2.2. Cost objective

This function (Eq. (9)) measures the cost (C) as a function of the unit prices (p_i) and the measurements (m_i). The construction units associated with the cost (rc) are the volume of concrete, the amount of post-tensioned steel, the amount of reinforcement steel, the area of the formwork and the CO_2 cost. Table 1 summarizes the unit prices obtained from the BEDEC database of the Institute of Construction Technology of Catalonia [30]. Note that the concrete unit price was determined from each mix design, including transport and placing. More details regarding unit prices and CO_2 emissions can be found in García-Segura et al. [22].

$$\mathrm{C}(\vec{x}) = \sum_{i=1,rc} p_i . m_i(\vec{x}) \qquad (9)$$

2.3. CO_2 emission objective

Emissions (E), measured in kg CO_2, were evaluated similarly to the economic cost. Life-cycle emissions are limited to the following stages: acquisition of raw materials, transport to the concrete plant, mixing, production of other materials, transport to the building site, construction activities and use stage. It is worth noting that there are other processes involve in the production and construction stage evaluation (e.g. cost of pavement, drainage and barriers, among others). However, the parameters that do not vary during the optimization process do not provide information about the optimum solutions. During use stage, carbon capture due to carbonation is considered. Maintenance activities are not included, since the durability constraints guarantee a service life of 100 years. Concrete unit emission is determined for each concrete grade from the aggregation of the concrete components. The unit emission takes into account the production and transport of each component, the concrete manufacture process, the concrete transport and the placement at the building site.

Unit emissions (e_i) are given in Table 1. The construction units associated with the emissions (re) are those of the cost, with the exception of the CO_2 cost. Carbonation was considered as a CO_2 capture, decreasing the embedded CO_2 emissions (Eq. (10)). The amount of CO_2 captured during the service life was estimated by García-Segura *et al* [22,31]. Eq. (11) estimates CO_2 capture as the product of the carbonation rate coefficient (k), the structure service life (T=100 years), the quantity of Portland cement per cubic meter of concrete (c), the amount of CaO content in Portland cement (CaO) (assumed to be 0.65), the proportion of calcium oxide that can be carbonated (p) (assumed to be 0.75), the exposed surface area of concrete (A), and the chemical molar fraction (M) (CO_2/CaO is 0.79). Table 2 provides the quantity of Portland cement per cubic meter and the carbonation rate coefficient according to f_{ck}. The carbonation rate coefficient depends on the exposure to rain. Only the bottom slab surface is considered to be protected from the rain.

$$\mathrm{E}(x) = \sum_{i=1,re} e_i . m_i(\vec{x}) - C_{co2}(\vec{x}) \qquad (10)$$

$$C_{co2}(\vec{x}) = k(\vec{x}) * \sqrt{T(\vec{x})} * c(\vec{x}) * CaO * p * A(\vec{x}) * M \qquad (11)$$

2.4. Overall safety factor objective

The overall safety factor (S) is calculated through the minimum safety factor (γ_j) for the ultimate limit states (Eq. (12)).

Torsion, flexure, transverse flexure and shear are taken into account. The factor γ_j is obtained as the ratio between the ultimate resistance of the structural response and the ultimate load effect of actions, considering the partial safety factors proposed by the code [32,33]. Thus, a safety coefficient of one implies strict compliance with the code.

$$S(\vec{x}) = Minimum\ \gamma_j(\vec{x}) \tag{12}$$

2.5. Structural analysis and verification

The structural object of this work is a three-span box-girder bridge, which is designed as a continuous girder bridge. A linear analysis by finite elements is performed. CSiBridge® and Matlab® software are used for the finite-element analysis and the limit states verification, respectively. In addition, the structural analysis and verification modules are embedded within the optimization process performed by Matlab®. Matlab® has been previously used to control parametric finite-element software [34]. The program is subdivided into eight modules as Fig. 3 illustrates. Module (1) updates the design variables according to the algorithm strategy. Then, module (2) completes the design and evaluates the section properties. Module (3) writes a $br document with the structure information, which will be later imported by CSiBridge®. In module (4), CSiBridge® runs the model. After the structural analysis, module (5) employs Application Programming Interface (API) functions to extract the results back to Matlab®. Next, module (6) processes the load effects from CSiBridge®, evaluates the bridge resistance, and checks the limit states. Once the structure is checked, module (7) evaluates the objective functions and module (8) obtains the Pareto optimum solutions. This process is repeated until the termination criterion is reached.

Shell elements are used for the accurate and efficient modeling of the PSC box-girder. Finite element (FE) mesh is based on the specifications of a maximum segment length for discretization information (3 m is considered) and a maximum submesh size (1.5 m is considered). The values considered for these parameters are determined with the aim of obtaining accurate results without compromising the computation time. In addition, every edge of the longitudinal and transverse section, like a change in thickness, is a condition for a FE division. Fig. 4 shows the finite element mesh. The reinforcing steel is modeled using a reinforcement grid, which is embedded in the shell element. The post-tensioned tendons are also incorporated in the model, with the curved shape defined by the variables. Actions take into account the traffic loads [33], the self-weight including the parapet (5 KN/m) and asphalt (24 KN/m^3), the thermal gradient [33], the post-tensioned steel effect and the differential settling in each support (5mm). Prestressing losses are considered at tensioning stage and final life. To this end, instantaneous losses due to friction, wedge penetration and elastic shortening of the concrete, and deferred losses are evaluated. A straight friction coefficient of 0.21, a coefficient of friction curve of 0.0013 and a penetration of the wedge of 5 mm are considered. The prestressing forces are evaluated at each section. Note that finite elements divide the deck in 40 sections.

Regarding the limit state verification, the geometrical and constructability requirements are also examined. Spanish codes [32,33], which have been adapted for the Eurocode content [35,36], are used. It is worth noting that the code [32] considers normal-strength concrete and high-strength concrete until 100 MPa. On this basis, the concrete strength variable can take values until 100 MPa. Special equation and limitations are considered for high-strength concrete following the code. Regarding ultimate limit states, shear, shear between web and flanges, flexure and torsion are studied. The durability conditions for a coastal environment demand the decompression limit state, the absence of cracking during prestressing and a concrete cover of 65 mm. Besides, the compressive stresses in the concrete cannot exceed 60% of the characteristic compressive strength. Note that these requirements affect the optimization problem. However, other specifications regarding the concrete quality, selection of raw materials, correct placing and curing of the concrete should be guaranteed for the durability conditions. The decompression must not occur in the concrete in the fibers located 100mm above and below the strands [35]. Regarding deflection, the instantaneous and time-dependent deflection with respect to the precamber was limited to 1/1400th of the main span length for the characteristic combination [32], and the frequent value for the live loads is limited to 1/1000th of the main span length [33]. As for the geometric and constructability requirements, the minimum separation between tendons and reinforcement [32] determines the minimum slab thickness. Other requirements as the anchorage lengths are considered. In addition, the authors propose some geometric constraints: the slope of the web must be greater than t_3/t_4, LR_2 cannot the greater than LR_1 and LR_3 cannot the greater than LR_2. It is worth noting that the optimization methodology do not follow usual

design rules where some variables depend on others to comply the limit states [14]. The heuristic optimization find the combination of the discrete and independent variables that minimizes or maximizes the objective functions.

2.6. Multiobjective harmony search

The harmony search algorithm, proposed by Geem et al. [37], is based on the process of searching for the perfect musical harmony. Several analogies are highlighted: the musical harmony with the solution vector, and a musician's improvizations with the stochastic random search. The harmony memory size (HMS) equivalent to the number of solution vectors, the harmony memory considering rate (HMCR), the pitch adjusting rate (PAR) and the maximum number of improvizations without improvement (IWI) are the algorithm parameters. A multiobjective version of the HS algorithm was proposed by Xu et al. [38] for the design of a reconfigurable mobile robot prototype. This paper uses a multiobjective harmony search based on the second proposal multiobjective harmony search of Ricart et al. [39]. These authors valued the performance of the algorithm from ZDT functions. Their performance metrics for experimental results showed that the algorithm was competitive even when compared to NSGA-II (Nondominated Sorting Genetic Algorithm II), which is one of the most representative algorithms for multiobjective optimization. Likewise, other authors [40-42] pointed out that multiobjective harmony search presented good results, including with regard to time. Fig. 5 shows the flowchart of the algorithm. The optimization procedure is as follows:

Step 1. Assign the algorithm parameters.

Step 2. Initialize the harmony memory (HM) with a population of HMS-feasible solution vectors. Vectors are obtained randomly from the discrete variable space. Vectors that correspond to feasible solutions are saved. Otherwise, solutions, which are not feasible, are discarded.

Step 3. Improvise a New Harmony Memory (NHM) with the same population as HM. The generation of a new harmony is based on random selection, memory consideration, and pitch adjustment. When a random number between 0 and 1 is less than the harmony memory considering rate (HMCR), the value of the variable is generated by the memory consideration, otherwise, it is obtained by a random selection. In the memory consideration, the value of decision variables xi is randomly selected from the harmony memory ($xi^l - xi^{\mathrm{HMS}}$). Then, this value will undergo a pitch adjustment with a probability of PAR. In this case, the value is modified one position up or down. This process is repeated for the total number of variables (m) and population.

Step 4. Update the harmony memory. The HM and the NHM are combined and confronted in the non-dominated sorting and ranking assignment method proposed by Fonsenca and Fleming [43]. The ranking of a solution (see Eq. 13) depends on the number of solutions which dominate the solution in question (n_d). The ranking is equal to the number of individuals that are dominated by plus one. Individuals on the Pareto front have a rank of 1 as they are not dominated.

$$rank(\vec{x}) = 1 + \mathrm{n}_d \tag{13}$$

Once the ranking is assigned to the 2*HMS solutions, the values are then scaled to score individuals in the population. The best solutions are selected to form the new HM with HMS solutions. The solutions with the lowest ranking are transferred firstly to HM. The procedure continues until the number of solutions with the next ranking is larger than the space of HM. In this time, the crowding distance metric is used. Instead of arbitrarily discarding some members, we use the diversity criterion based on the highest crowding distance. The measure of the crowding distance indicates the density of the solution vectors surrounding a particular solution vector. This quantity is estimated by the perimeter of the cuboid formed by the nearest neighbors in the objective space as the vertices (see Equation (14)). The crowding distance of a solution (j) is evaluated as the distance to the neighbors (j+1/j-1) sorted for each objective (m). The solutions with the greatest values of crowding distance are transferred to HM to complete it. This criterion benefits the diversity.

$$d_{I_j^m} = d_{I_j^m} + \frac{f_m^{I_{j+1}^m} - f_m^{I_{j-1}^m}}{f_m^{max} - f_m^{min}} \tag{14}$$

Step 5. Stopping criterion. The procedure ends when the number of sequential improvizations without improvement reaches the maximum improvizations without improvement (IWI).

To improve the solution quality, diversification and intensification strategies are combined. Firstly, the use of crowding distance ensures a spread of solutions on the Pareto-optimal front. Secondly, three phases of HM parameters are carried out to progressively reduce the randomness, and consequently, move from a

diversification to an intensification strategy. The combination of both strategies promotes firstly the exploration of the entire space, and later, converges on the best design. The appropriate incorporation of these two counterbalancing components is vital for the efficiency of the algorithm [44]. After five harmony memory updates without improvement (Step 4), there is a phase transition.

Phase 1: PAR=0.4, HMCR=0.7, HMS=50

Phase 2: PAR=0.4, HMCR=0.7, HMS=50, fix the memory consideration

Phase 3: PAR=0.4, HMCR=1, HMS=50, fix the memory consideration

The parameters of Phase 1 are selected according to the Design of Experiments methodology [22]. A harmony memory size of 50 solutions captures the variability of solutions, reduces the computation time and ensures the quality of solutions. As the algorithm progresses, HMS is increased to the number of Pareto solutions provided that the number of solutions with ranking equal to one is greater than the value of HMS. In Phase 1, the memory consideration can select the values of the variables from different solutions of the HM. In contrast, Phase 2 fixes the memory consideration to a unique random HM solution. Therefore, the movement is done around one random solution. In Phase 3, the value of HMCR is equal to 1, which means that the random selection is eliminated. At this point of the algorithm, finding a better random design is less likely. Therefore, a refinement process of local solutions is carried out. Finally, the algorithm ends when the harmony memory is unchanged during a number of IWI equal to ten.

3. Results

Fig. 6 shows the Pareto set for the three objectives. The Pareto set selects the solutions whose objective values cannot be improved without worsening the value of at least one objective. Commonly, the Pareto set of solutions regarding three objectives forms a surface where each solution improves one objective. However, in this case, solutions stand nearly in a line. Cost and emission objectives are not totally in conflict. On one hand, the results show that these objectives are closely related: reducing the material consumption reduces, in turn, both objectives. But on the other hand, unit prices and emissions are not in any proportional relationship to one another. For instance, the concrete strength increment has a greater impact on the CO_2 emissions than the cost, since cement is a carbon-intensive material.

The relationship between cost, emission and safety shows whether variables are more influenced by the safety requirements or the differences between unit costs and emissions. Designs of road bridges are correlated with the heavy traffic loads. Findings suggest that structural efficiency has a great impact on the optimum design. Besides, cost optimization leads to a reduction in material consumption and, therefore, this criterion is a good approach to achieve an environmentally friendly design. While objectives are in conflict for random solutions, they are close to each other near their optima. Thus, as the algorithm progresses, cost and emission objectives show stronger relationships.

In addition, the benefits of combining diversification and intensification are illustrated in Fig. 6. The parameters used for Phase 1 allow the exploration of the search space, and spread the solutions along the objective functions. The diversity of the population is essential for a multiobjective optimization. After five memory updates without improvement, the memory consideration is fixed to one random solution (Phase 2), and consequently, the combination of solutions is eliminated. The algorithm improves the solution quality by generating new designs from parts of existing designs in the HM, and a random and mutation component. The cheapest solutions are improved in both cost and overall safety factor. Phase 3 achieved solutions with a 13% and 18% reduction in cost and emissions compared to Phase2, by intensifying the solutions using only the PAR to perturb members. Note that 1800, 1000 and 1700 feasible solutions are evaluated during Phase 1, Phase 2 and Phase 3, respectively. The computation time for obtaining an exact feasible is about 1500 s, mainly due to the finite element analysis and output the results. Population algorithms enable the use of parallelization techniques to reduce the computation time. In this case, the new harmony vectors can be checked in different computers and returned to the master to update the harmony memory.

Fig. 7 shows that the minimum cost coincides with the minimum emission solution. These objectives present a good linear fit (E=2.3383C-206773.16) with a regression coefficient (R^2) equal to 0.99689. The results indicate that when cost increases by one euro, the CO_2 emissions rise by 2.34 kg. This relationship can therefore be used as a correspondence between the objectives in the following analysis. In addition, results show that cost optimization is a good approach for emission minimization regardless of the safety level. García-Segura et al. [22] carried out a parametric study of the span length. They also found that optimal solutions in terms of monetary costs have quite satisfactory environmental results. This paper extends this outcome to the transverse effect, since the overall safety factor also considers the transverse flexure limit state. This statement could be also obtained by a parametric study of the width in a mono-

objective optimization.

Regarding the overall safety factor, results show that increasing safety conditions entails an increase in the cost. However, this increment is not constant. Firstly, the overall safety factor is improved without a high cost increment. Fig. 8 shows a linear relation between both objectives until C=450,000 € and S=1.4 (S=9.2525E-06C-2.7423 with a regression coefficient R^2=0.90971). This means that 10,808 € are needed to increase the overall safety factor by 10%. Then, the safety increment is more expensive. The general trend is described by a linear relation (S=1.018E-06C+0.96467 with a regression coefficient R^2=0.95084) until C=750,000 € and S=1.69. Increasing the overall safety factor by 10% results in a cost increment of 98,232 €. Finally, the overall safety factor hardly increases, even if the cost increases. A linear relation between both objectives can be highlighted (S=1.6992E-07C+1.5664 with a regression coefficient R^2=0.95176). Where the emissions are concerned, the trend is the same considering the correspondence between cost and emissions.

Fig. 9 illustrates a box-plot for the variables of the optimum solutions. The analysis of the figure reveals the variables which should be increased to improve safety The percentiles [25^{th}, 50^{th}, 75^{th}] of the web inclination width (d) are [0.5 m, 0.6 m, 0.8 m]. These values correspond to a web slope range between 3.5 and 4. The slope, considered as the ratio between the width and the depth, remains approximately constant, since both the depth and the web inclination width increases in parallel to improve safety. The width of the bottom slab (b) presents values from 4.4 to 5.3 m, which is equivalent to a ratio of 0.37 and 0.45 of the width of the deck. The median value is 0.38. This means that 50% of values range from ratios of 0.37 to 0.38 the width of the deck. Only when the required overall safety factor is high, should the width of the bottom slab be increased to decrease the flange length and, consequently, the transverse flexure demand.

Regarding the depth (h), the minimum value is 2.3m and the interquartile range varies from 2.35 to 3.5 m. This corresponds to a relationship between the main span length and the depth of 19.1, 18.7 and 12.6, respectively. Fomento [45] recommends a ratio L/h of between 18 and 20 for this type of bridge. Therefore, the optimum bridge in terms of cost has a depth within the range proposed by the guidance document, even if the case study is located in a coastal region. To guarantee the decompression limit state, the depth is increased to increase, in turn, the inertia and reduce the stresses.

The thicknesses e_s, e_v and e_i range between 0.25 and 0.4 m. Most of the designs adopt a thickness of the top slab between 0.25 and 0.3. This indicates that increasing e_s is not advisable to improve structural safety, since it results in an additional weight. With regard to the thickness of the external flange, almost 50% of the values are 0.25 m and the other 50% are 0.3 m. As for the thickness of the bottom slab, the percentiles are [0.3 m, 0.35 m, 0.4 m]. Increasing this thickness improves the flexure capacity over the supports. The thickness of the webs (e_a) shows a narrow interquartile range from 0.55 to 0.6 m. Even the thickness of the webs has an influence on the shear, this is not the most economic variable to increase the shear resistance. The thickness of the internal flange section presents values between 0.4 and 0.55 m. Transverse flexure impacts especially over the top slab, which is mainly affected by traffic loads. While it is not advisable to increase the thickness of the top slab, the thickness of the internal flange section is worth increasing to improve the transverse flexure.

Concerning the concrete strength (f_{ck}), 50% of the values take the 35 Mpa grade, which is the minimum proposed. Although there is an outlier solution of 55MPa, results suggest that increasing the concrete grade is not the best solution to improve safety. The use of high-strength concrete may lead to a reduction in depth or amount of reinforcement. However, the constraints regarding serviceability limit states and minimum amount of reinforcement restrict these variables. As for the post-tensioned steel, the interquartile range of the number of strands varies from 194 to 256. Firstly, post-tensioned steel is adjusted to verify the decompression limit state. Afterwards, this variable is increased to contribute to the flexure capacity. The 25^{th} percentile and median value of the distance from the piers to the point of inflection (L_{pi}) are equal to 0.1, the span length. This value provides good results for most of the overall safety factors. As this distance is reduced, the post-tensioned steel effect in the piers is intensified. Finally, a ratio of 0.5 of half of the bridge depth is an adequate value for the eccentricity in the external spans (e_p) to balance the stresses.

Flexure, shear, torsion and transverse flexure are the limit states taken into account to evaluate the overall safety factor. The evolution of these limit states indicates which are restrictive. Optimization, unlike the traditional design, seeks the value of the variables that minimizes all the limit states. Only the limit states whose influential variables are also variables of a most restrictive limit state, are not critical. This is the case of flexure (see Fig. 10). Flexure factors adopt values around 1.4 until the overall safety factor reaches this value. This means that the variables affecting the flexure factor are conditioned by a more restrictive limit state. Results suggest that the decompression limit state is the one with the greater influence over

variables such as depth and number of strands. After that, the flexure factor is put on a par with the overall safety criteria, which indicates that flexure is a restrictive factor.

Analyzing the values of the variables with respect to the safety improvement, it is worth noting the variables with a clear relationship. The concrete volume (see Fig. 11), the post-tensioned steel (see Fig. 12), and the longitudinal reinforcing steel (see Fig. 13) show nearly constant values until the 1.4 overall safety factor and any increment after that. It is worth noting that the depth and the post-tensioned steel are correlated to guarantee the decompression limit state. While both variables increase in steps, the longitudinal reinforcement is adjusted incrementally to achieve the overall safety factor required. Increasing the depth and the number of strands is just an economic alternative when it involves a large decrease in the longitudinal reinforcing steel, as it happens around the 1.54 safety factor. The transverse reinforcing steel (see Fig. 14), as it is influenced by shear, torsion and transverse flexure, has a progressive increment. The results suggest that to increase the overall safety factor to 1.4, the transverse reinforcement is mainly increased, and this has a little influence on the cost. From this point on, an increment in the longitudinal reinforcement, the post-tensioned steel, and the concrete volume (mainly due to the depth) are also needed, which entail high prices. Findings indicate that a bridge designer can improve the safety with a little cost increment by choosing the correct design variables.

Comparing the optimum solution in terms of cost with Fomento [45], the amount of reinforcement per surface of deck (66.89 kg/m^2) is smaller than the code suggestion (between 90 and 110 kg/m^2). However, the concrete volume per surface of deck (0.67 m^3/m^2) and the amount of post-tensioned steel per surface of deck (21.98 kg/m^2) are greater. Fomento [45] recommends a concrete volume between 0.5 and 0.56 m^3/m^2 and an amount of post-tensioned steel between 13 and 19 kg/m^2 for this span length. Note that the optimization problem involves a bridge in a coastal region with restricting serviceability limit states, which lead to greater cross-sections and post-tensioned steel. Considering the cost of concrete, reinforcing and post-tensioned steel, the optimum solution reduces the cost by 3% and 14%, and the CO_2 emissions by 6% and 16%, compared to the average and maximum measurements proposed by the guidance document. These values are obtained from the most economical solution, which uses 35 MPa concrete. Therefore, the heuristic optimization found a cheaper and more environmentally friendly bridge, reducing the reinforcing steel but increasing the concrete volume and post-tensioned steel.

4. Concluding remarks

This research presented a multiobjective optimization of post-tensioned concrete box-girder road bridges. The design is formulated as an optimization of cost, CO_2 emissions, and overall safety factor. A computer tool, suitable for optimizing real-bridge problems, linked CSiBridge® and Matlab® software to integrate finite-element analysis, limit state verification, and multiobjective optimization. The analysis was performed through shell elements, which incorporated the reinforcing steel as a reinforcement grid and post-tensioned tendons. The best combination of variables, which involves the geometry, concrete strength, reinforcing and post-tensioned steel, was defined through a multiobjective harmony search algorithm, with a combination of diversification and intensification strategies. This task was carried out by firstly exploring random locations in the search space, and later concentrated on a refinement process around good solutions.

The analysis of the results reveals the relation between objectives, the best variables to improve safety, and the critical ultimate limit states. Results show that cost optimization is a good approach to achieve an environmentally friendly design, as long as cost and CO_2 emission criteria lead to a reduction in material consumption. Besides, this outcome is maintained regardless of the safety level. While objectives are in conflict for random solutions, they are close to each other near their optima. Decreasing the cost by one euro reduces the CO_2 emissions by 2.34 kg. Regarding the overall safety factor, three linear relations between cost and this objective are highlighted. To increase the overall safety factor from 1 to 1.4, costs increase from 400,000 € to 450,000 €. After this point, the safety improvement results are more expensive.

The optimum values of the variables depend on the parameters selected for the case study, like the width and span length. However, the inclusion of the safety function provides vital knowledge about the dependence of the variables to the safety level. The decompression limit state is a restricting limit state that conditions variables such as depth and number of strands. The analysis of the Pareto front reveals the variables with smaller influence over the cost and emissions, which are better for improving safety. The depth, together with the thickness of the bottom slab, the post-tensioned steel, and the longitudinal reinforcing are the main variables providing the flexure capacity. Results indicate that the increment in concrete grade and the thickness of the top slab are not the best solutions to improve safety. The thickness of the internal flange section should be increased and the flange length should be decreased to improve the

transverse flexure performance. The slope of the web inclination remains approximately constant for all the overall safety factors. The thickness of the webs is not the most economic variable to increase the shear resistance. Comparing the best cost result with the standards, the tool found a cheaper and a more environmentally friendly bridge, by reducing the reinforcing steel but increasing the concrete volume and post-tensioned steel.

Acknowledgments

The authors acknowledge the financial support of the Spanish Ministry of Economy and Competitiveness, along with FEDER funding (BRIDLIFE Project: BIA2014-56574-R) and the Research and Development Support Program of Universitat Politècnica de València (PAID-02-15).

References

[1] Barr AS, Sarin SC, Bishara AG. Procedure for structural optimization. ACI Struct J 1989;86:524-31.

[2] Aguilar RJ, Movassaghi K, Brewer JA, Porter JC. Computerized optimization of bridge structures. Comput Struct 1973;3:429-42. doi:10.1016/0045-7949(73)90089-8.

[3] Rabbat BG, Russell HG. Optimized sections for precast prestressed bridge girders. PCI J 1982;27:88-108.

[4] Lounis Z, Cohn MZ. Optimization of precast prestressed concrete bridge girder systems. PCI J 1993;38:60-78.

[5] Wills J. A mathematical optimization procedure and its application to the design of bridge structures. Transport and Road Research Laboratory. Report LR_{555}. Wokingham, UK; 1973.

[6] Bond D. An examination of the automated design of prestressed concrete bridge decks by computer. Proc Inst Civ Eng 1975;59:669-97. doi:10.1680/iicep.1975.3634.

[7] Yu. CH, Gupta. NC Das, H. Paul. Optimization of prestressed concrete bridge girders. Eng Optim 1986;10:13-24. doi:10.1080/03052158608902524.

[8] Hare W, Nutini J, Tesfamariam S. A survey of non-gradient optimization methods in structural engineering. Adv Eng Softw 2013;59:19-28. doi:10.1016/j.advengsoft.2013.03.001.

[9] Lagaros ND, Fragiadakis M, Papadrakakis M, Tsompanakis Y. Structural optimization: A tool for evaluating seismic design procedures. Eng Struct 2006;28:1623-33. doi:10.1016/j.engstruct.2006.02.014.

[10] Srinivas V, Ramanjaneyulu K. An integrated approach for optimum design of bridge decks using genetic algorithms and artificial neural networks. Adv Eng Softw 2007;38:475-87. doi:10.1016/j.advengsoft.2006.09.016.

[11] Perea C, Alcala J, Yepes V, Gonzalez-Vidosa F, Hospitaler A. Design of reinforced concrete bridge frames by heuristic optimization. Adv Eng Softw 2008;39:676-88. doi:10.1016/j.advengsoft.2007.07.007.

[12] Martínez-Martín FJ, González-Vidosa F, Hospitaler A, Yepes V. A parametric study of optimum tall piers for railway bridge viaducts. Struct Eng Mech 2013;45:723-40.

[13] Rana S, Islam N, Ahsan R, Ghani SN. Application of evolutionary operation to the minimum cost design of continuous prestressed concrete bridge structure. Eng Struct 2013;46:38-48. doi:10.1016/j.engstruct.2012.07.017.

[14] Martí J V., Gonzalez-Vidosa F, Yepes V, Alcalá J. Design of prestressed concrete precast road bridges with hybrid simulated annealing. Eng Struct 2013;48:342-52. doi:10.1016/j.engstruct.2012.09.014.

[15] Martí J V., Yepes V, González-Vidosa F. Memetic algorithm approach to designing precast-prestressed concrete road bridges with steel fiber reinforcement. J Struct Eng 2015;141:04014114. doi:10.1061/(ASCE)ST.1943-541X.0001058.

[16] Alberdi R, Murren P, Khandelwal K. Connection topology optimization of steel moment frames using metaheuristic algorithms. Eng Struct 2015;100:276-92. doi:10.1016/j.engstruct.2015.06.014.

[17] Camp C V., Huq F. CO2 and cost optimization of reinforced concrete frames using a big bang-big crunch algorithm. Eng Struct 2013;48:363-72. doi:10.1016/j.engstruct.2012.09.004.

[18] Paya-Zaforteza I, Yepes V, Hospitaler A, González-Vidosa F. CO_2-optimization of reinforced concrete frames by simulated annealing. Eng Struct 2009;31:1501-8. doi:10.1016/j.engstruct.2009.02.034.

[19] Yepes V, Gonzalez-Vidosa F, Alcala J, Villalba P. CO2-optimization design of reinforced concrete retaining walls based on a VNS-threshold acceptance strategy. J Comput Civ Eng 2012; 26(3):378–86. doi: 10.1061/(ASCE)CP.1943-5487.0000140.

[20] Camp C V., Assadollahi A. CO_2 and cost optimization of reinforced concrete footings subjected to uniaxial uplift. J Build Eng 2015;3:171-83. doi:10.1016/j.jobe.2015.07.008.

[21] Yepes V, Martí J V., García-Segura T. Cost and CO_2 emission optimization of precast–prestressed concrete U-beam road bridges by a hybrid glowworm swarm algorithm. Autom Constr 2015;49:123-34. doi:10.1016/j.autcon.2014.10.013.

[22] García-Segura T, Yepes V, Alcalá J, Pérez-López E. Hybrid harmony search for sustainable design of post-tensioned concrete box-girder pedestrian bridges. Eng Struct 2015;92:112-22. doi:10.1016/j.engstruct.2015.03.015.

[23] de Medeiros GF, Kripka M. Optimization of reinforced concrete columns according to different environmental impact assessment parameters. Eng Struct 2014;59:185-94. doi:10.1016/j.engstruct.2013.10.045.

[24] García-Segura T, Yepes V, Martí JV, Alcalá J. Optimization of concrete I-beams using a new hybrid glowworm swarm algorithm. Lat Am J Solids Struct 2014;11:1190-205. doi:10.1590/S1679-78252014000700007.

[25] Zavala GR, Nebro AJ, Luna F, Coello Coello CA. A survey of multi-objective metaheuristics applied to structural optimization. Struct Multidiscip Optim 2013;49:537-58. doi:10.1007/s00158-013-0996-4.

[26] Liu M, Frangopol DM. Multiobjective maintenance planning optimization for deteriorating bridges considering condition, safety, and life-cycle cost. J Struct Eng 2005;131:833-42. doi:10.1061/(ASCE)0733-9445(2005)131:5(833).

[27] Paya I, Yepes V, González-Vidosa F, Hospitaler A. Multiobjective optimization of reinforced concrete building frames by simulated annealing. Comput Civ Infrastruct Eng 2008;23:596-610. doi:10.1111/j.1467-8667.2008.00561.x.

[28] Quaglia CP, Yu N, Thrall AP, Paolucci S. Balancing energy efficiency and structural performance through multi-objective shape optimization: Case study of a rapidly deployable origami-inspired shelter. Energy Build 2014;82:733-45. doi:10.1016/j.enbuild.2014.07.063.

[29] Yepes V, García-Segura T, Moreno-Jiménez JM. A cognitive approach for the multi-objective optimization of RC structural problems. Arch Civ Mech Eng 2015;15:1024-36. doi:10.1016/j.acme.2015.05.001.

[30] BEDEC. Institute of Construction Technology of Catalonia. Barcelona, Spain n.d. www.itec.cat. [10.08.14].

[31] García-Segura T, Yepes V, Alcalá J. Life cycle greenhouse gas emissions of blended cement concrete including carbonation and durability. Int J Life Cycle Assess 2014;19:3-12.

doi:10.1007/s11367-013-0614-0.

[32] Fomento M. EHE-08: Code on structural concrete. Madrid, Spain: Ministerio de Fomento; 2008.

[33] Fomento M. IAP-11: Code on the actions for the design of road bridges. Madrid, Spain: Ministerio de Fomento; 2011.

[34] Alegria Mira L, Filomeno Coelho R, Thrall AP, De Temmerman N. Parametric evaluation of deployable scissor arches. Eng Struct 2015;99:479-91. doi:10.1016/j.engstruct.2015.05.013.

[35] European Committee for Standardisation. EN1992-2:2005. Eurocode 2: Design of concrete structures- Part 2: Concrete bridges. Design and detailing rules. Brussels; 2005.

[36] European Committee for Standardisation. EN 1991-2:2002. Eurocode 1: Actions on structures. Part 2: Traffic loads bridges; 2002.

[37] Geem Z, Kim, J.H.Loganathan GV. A new heuristic optimization algorithm: harmony search. Simulation 2001;76:60-8.

[38] Xu H, Gao XZ, Wang T, Xue K. Recent advances in harmony search algorithm. In: Geem ZW, editor., Berlin, Heidelberg: Springer Berlin Heidelberg; 2010, p. 11-22. doi:10.1007/978-3-642-04317-8_2.

[39] Ricart J, Hüttemann G, Lima J, Barán B. Multiobjective harmony search algorithm proposals. Electron Notes Theor Comput Sci 2011;281:51-67. doi:10.1016/j.entcs.2011.11.025.

[40] Sivasubramani S, Swarup KS. Multi-objective harmony search algorithm for optimal power flow problem. Int J Electr Power Energy Syst 2011;33:745–52. doi:10.1016/j.ijepes.2010.12.031.

[41] Hajipour V, Rahmati SHA, Pasandideh SHR, Niaki STA. A multi-objective harmony search algorithm to optimize multi-server location–allocation problem in congested systems. Comput Ind Eng 2014;72:187–97. doi:10.1016/j.cie.2014.03.018.

[42] Pavelski LM, Almeida CP, Goncalves RA. Harmony search for multi-objective optimization. IEEE Brazilian Symposium on Neural Networks; 2012, p. 220–5. doi:10.1109/SBRN.2012.19.

[43] Fonseca CM, Fleming PJ. Genetic algorithms for multiobjective optimization: Formulation, discussion and generalization 1993:416-23.

[44] Murren P, Khandelwal K. Design-driven harmony search (DDHS) in steel frame optimization. Eng Struct 2014;59:798-808. doi:10.1016/j.engstruct.2013.12.003.

[45] Fomento M. New overpasses: general concepts. Madrid, Spain: Ministerio de Fomento; 2000.

Table 1. Unit prices and CO_2 emissions considered in the PSC box-girder road bridge

Unit measurements	**Cost (€)**	**Emission ($kgCO_2$)**
m^2 of formwork	33.81	2.08
kg of steel (B-500-S)	1.16	3.03
kg of prestressing steel (Y1860-S7)	3.40	5.64
m^3 of concrete HP-35	104.57	321.92
m^3 of concrete HP-40	109.33	338.90
m^3 of concrete HP-45	114.10	355.88
m^3 of concrete HP-50	118.87	372.86
m^3 of concrete HP-55	123.64	389.84
m^3 of concrete HP-60	128.41	406.82
m^3 of concrete HP-70	137.95	440.78
m^3 of concrete HP-80	147.49	474.74
m^3 of concrete HP-90	157.02	508.70
m^3 of concrete HP-100	166.56	542.66
t CO_2 emission	5.00	

Table 2. Concrete design properties

Unit	***k* exposed to rain ($mm/year^{0.5}$)**	***k* protected from rain ($mm/year^{0.5}$)**	**Cement (kg/m^3)**
m^3 of concrete HP-35	1.50	3.01	300
m^3 of concrete HP-40	1.25	2.50	320
m^3 of concrete HA-45	1.05	2.11	350
m^3 of concrete HP-50	0.90	1.81	400
m^3 of concrete HP-55	0.79	1.57	457
m^3 of concrete HP-60	0.69	1.38	485
m^3 of concrete HP-70	0.55	1.09	493
m^3 of concrete HP-80	0.45	0.89	497
m^3 of concrete HP-90	0.37	0.74	517
m^3 of concrete HP-100	0.31	0.63	545

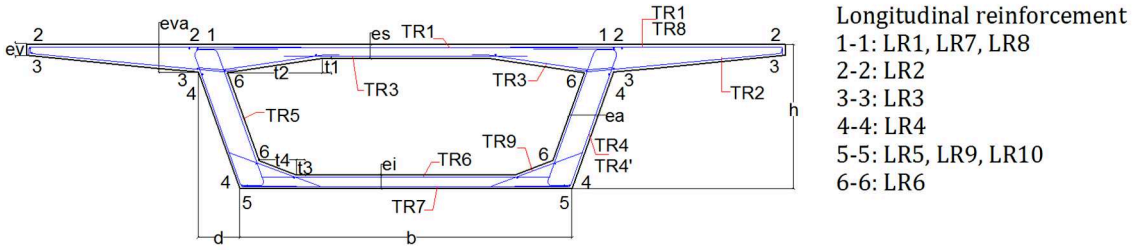

Fig. 1. Bridge design: Geometry and reinforcing steel.

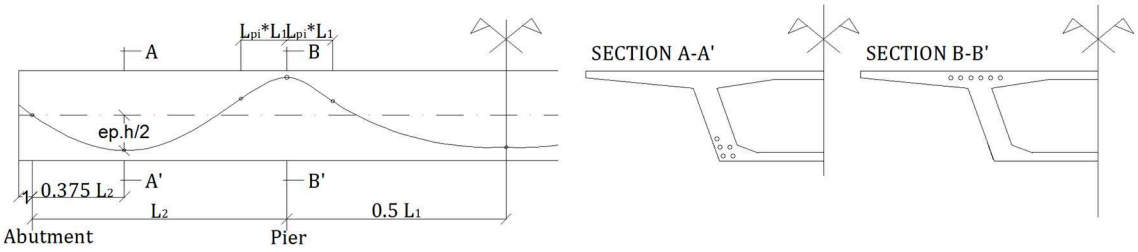

Fig. 2. Bridge design: Post-tensioned steel.

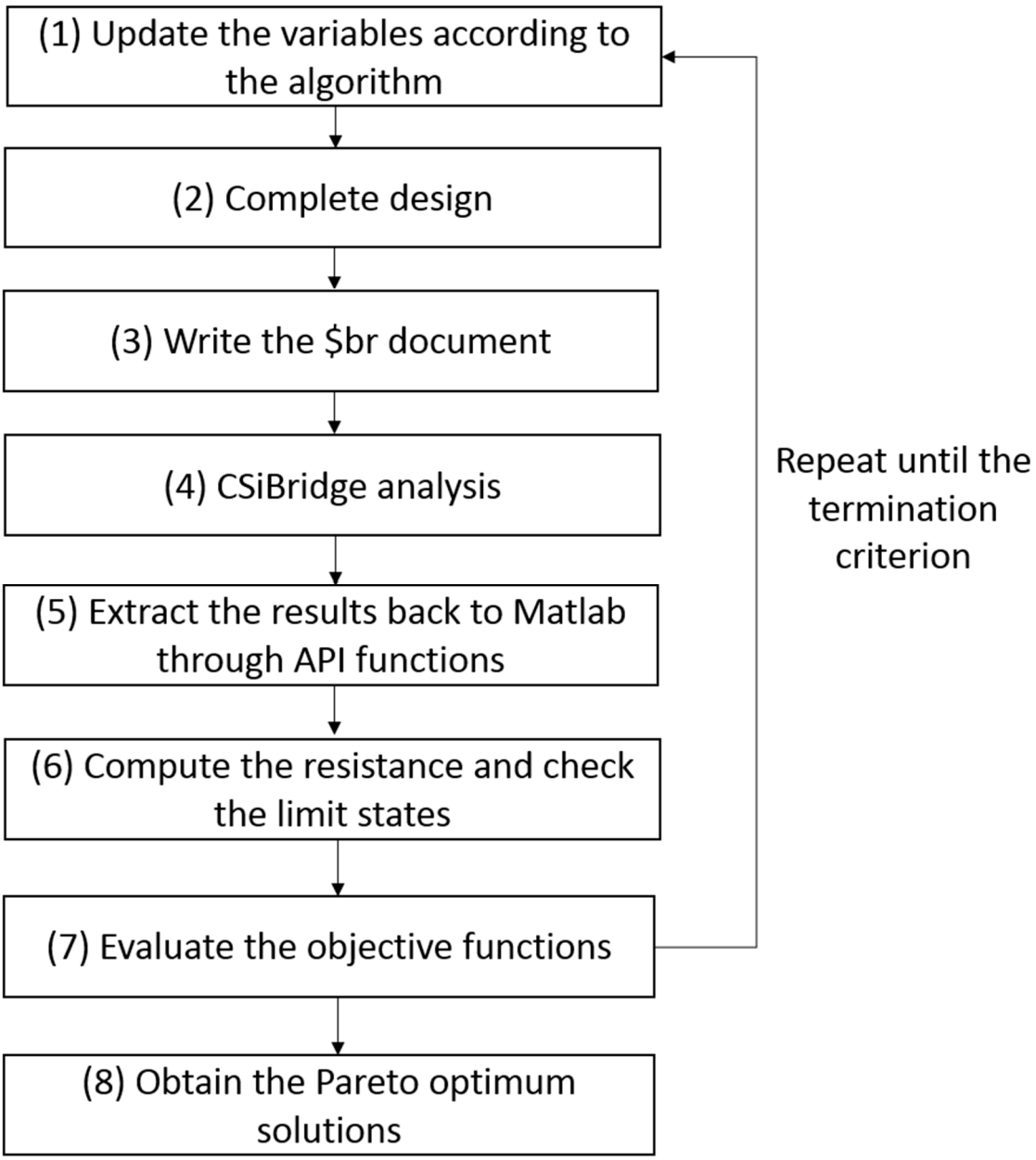

Fig. 3. Flowchart for structural analysis and optimization.

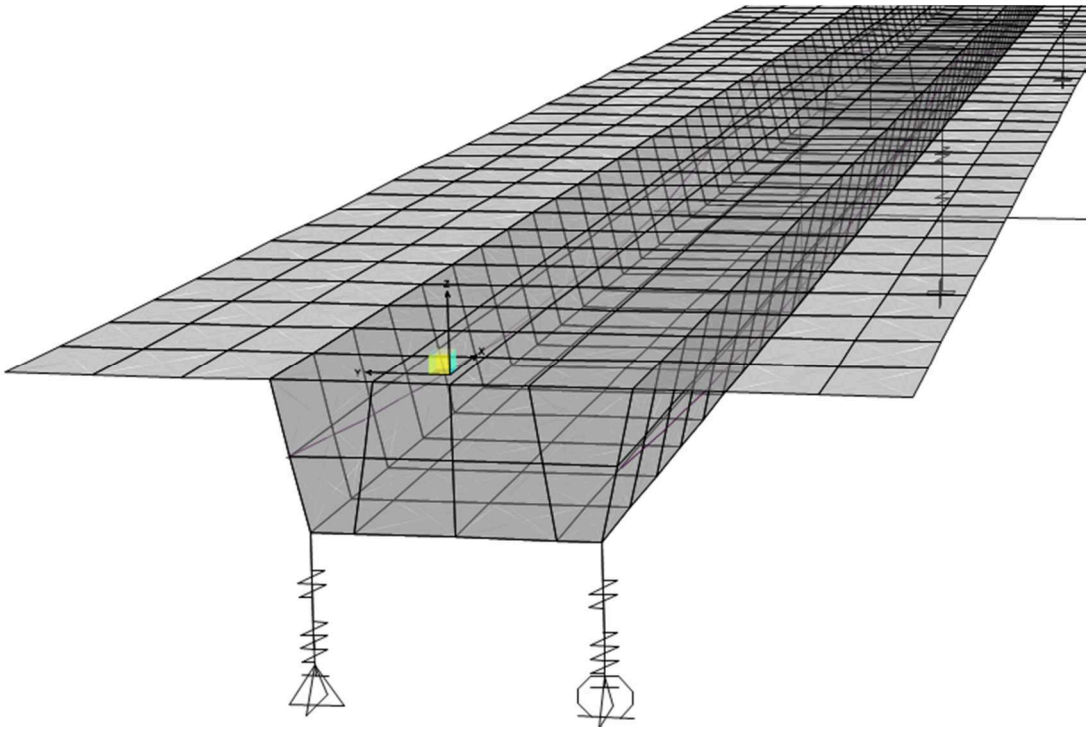

Fig. 4. Finite element mesh.

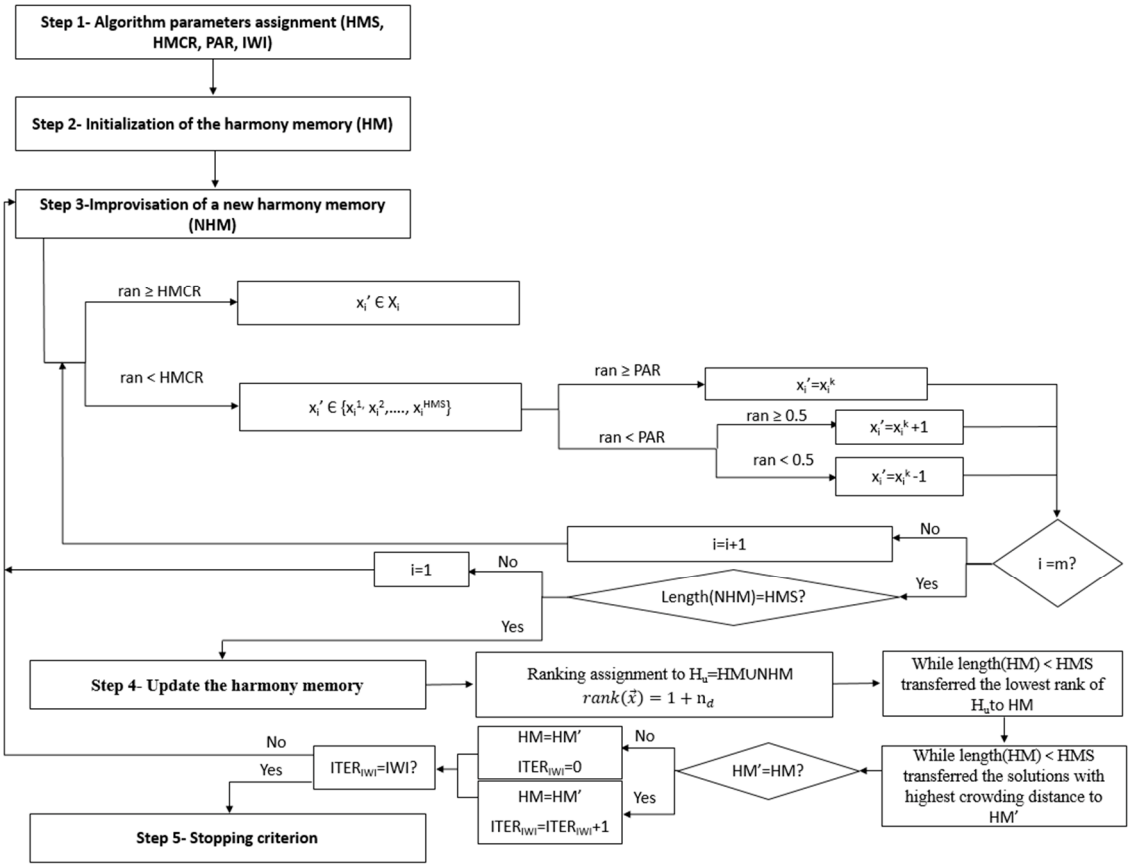

Fig. 5. Flowchart of multiobjective harmony search.

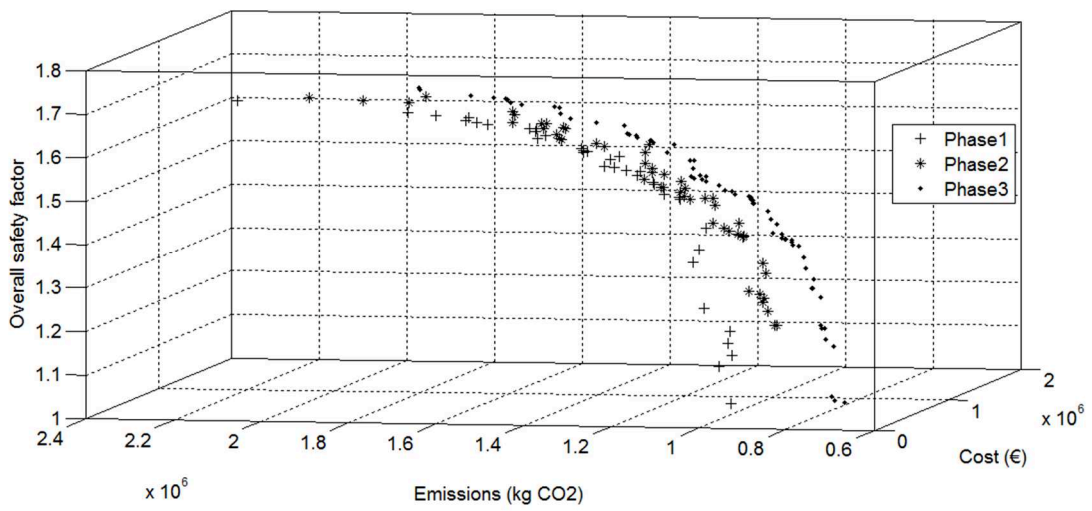

Fig. 6. Multiobjective harmony search evolution.

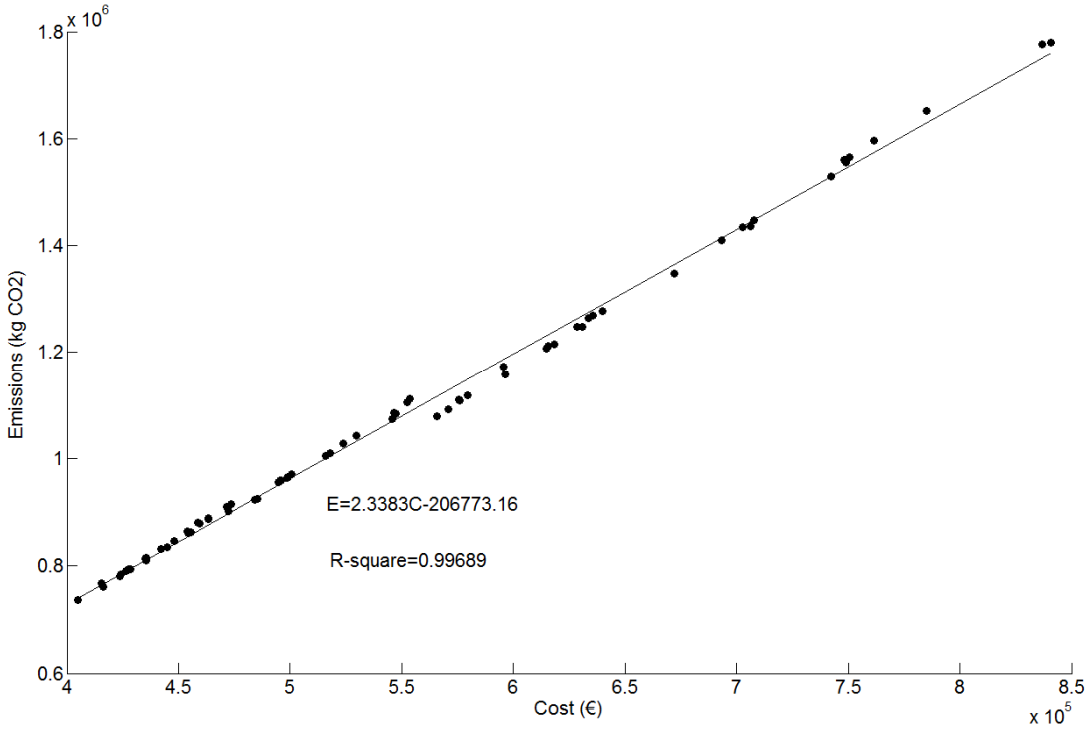

Fig. 7. Pareto set of solutions for cost and CO_2 emissions.

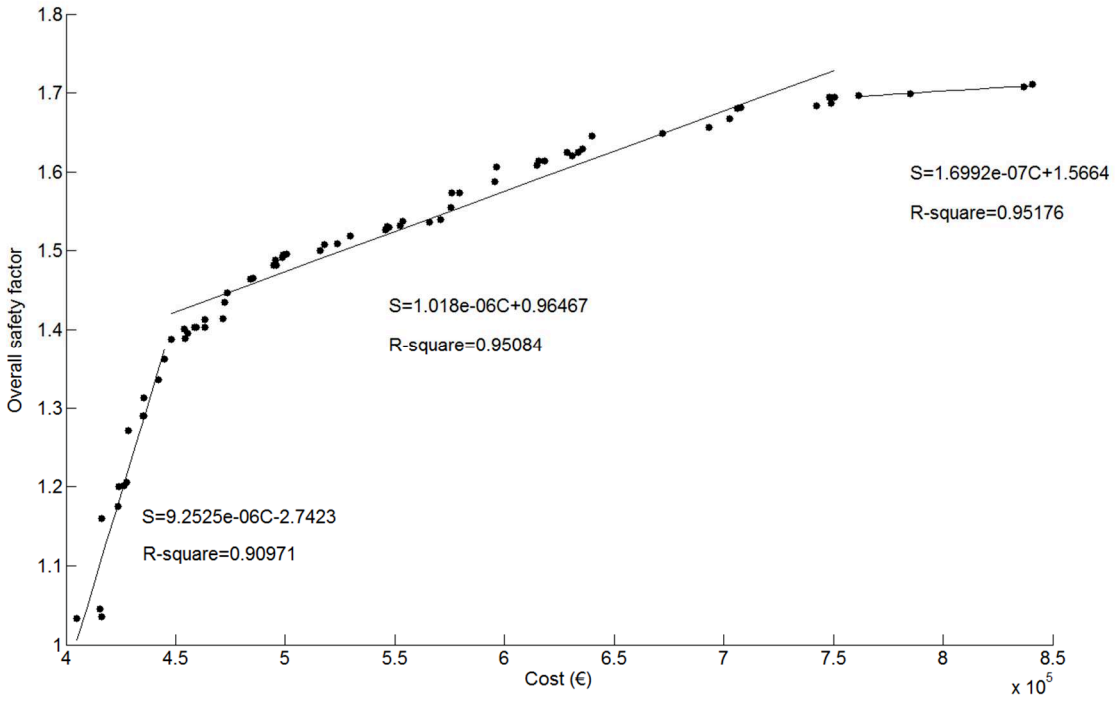

Fig. 8. Pareto set of solutions for cost and overall safety factor.

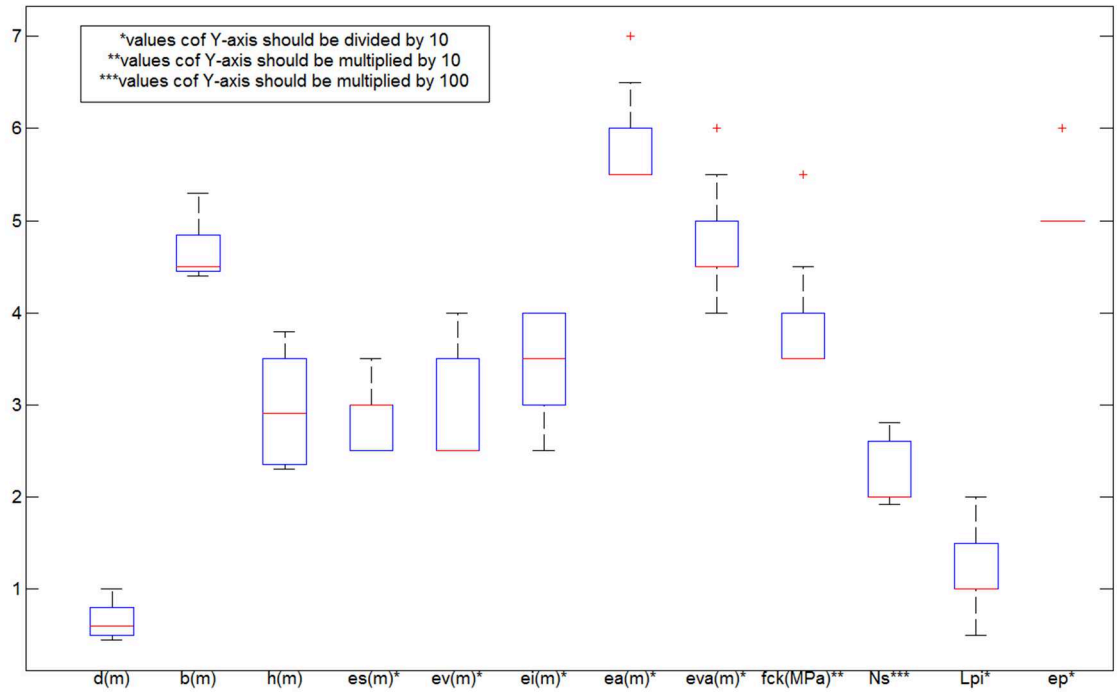

Fig. 9. Box-plot of the design variables of Pareto solutions.

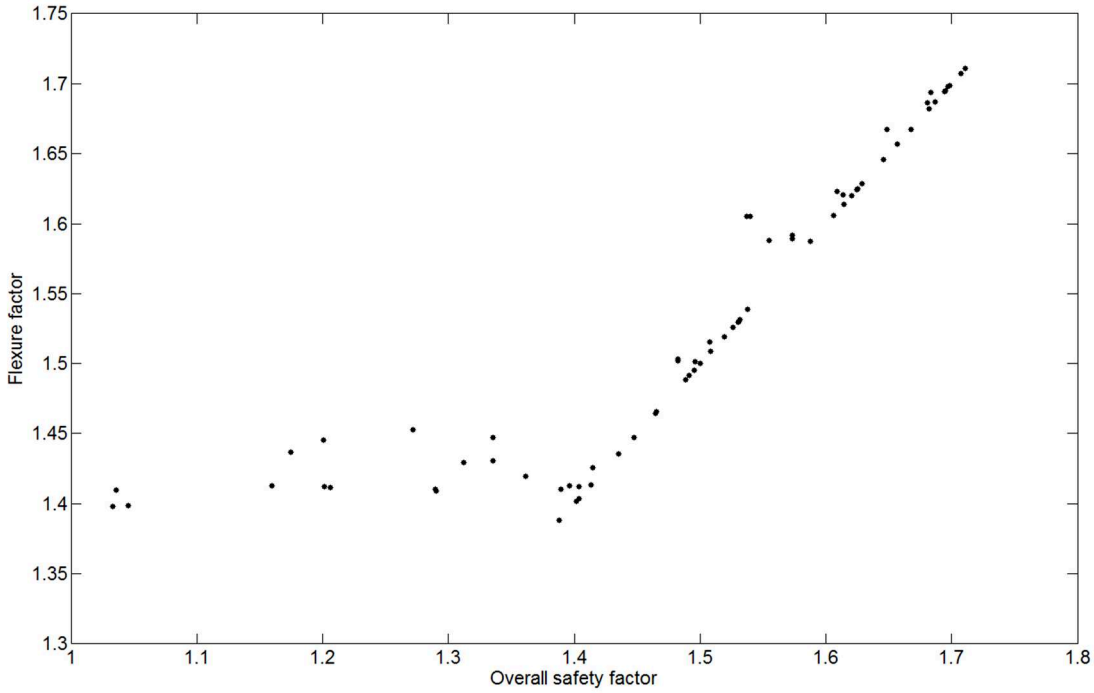

Fig. 10. Relation between flexure factor and overall safety factor.

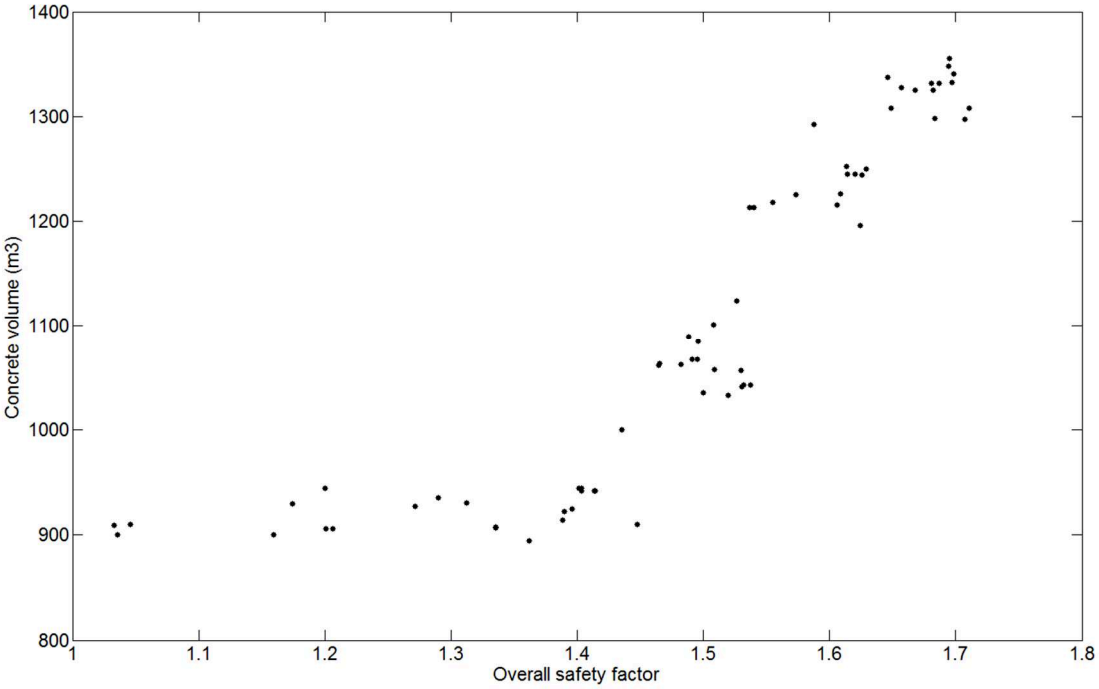

Fig. 11. Volume of concrete according to overall safety factor.

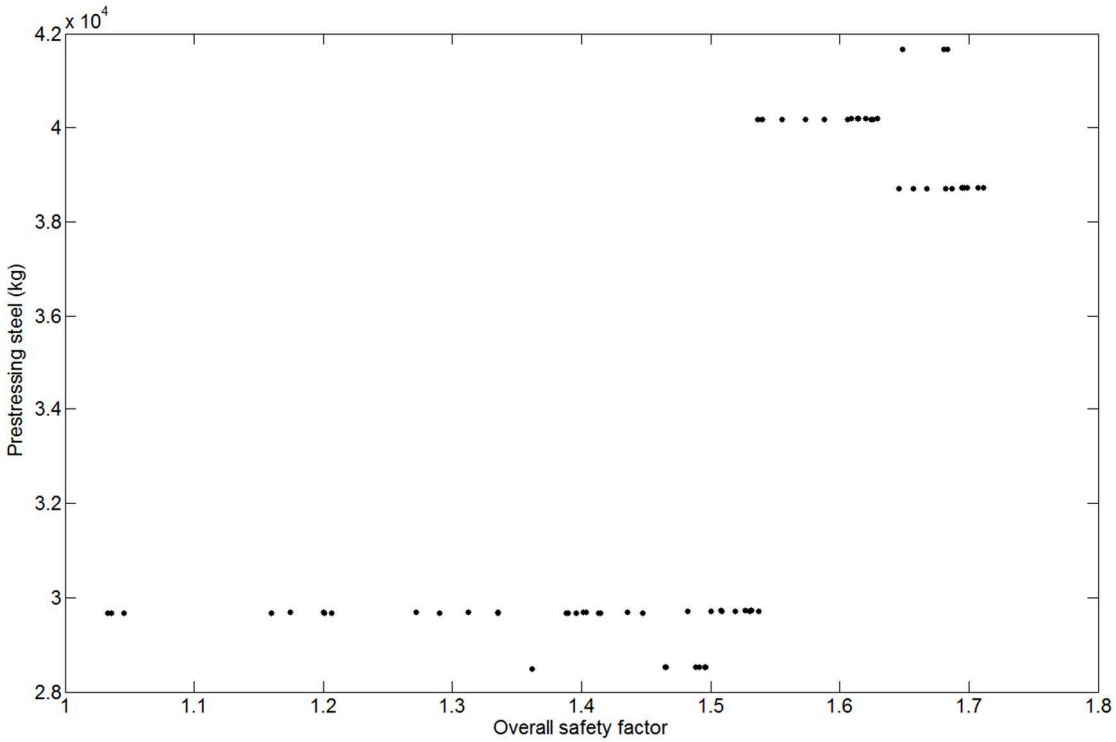

Fig. 12. Amount of post-tensioned steel according to overall safety factor.

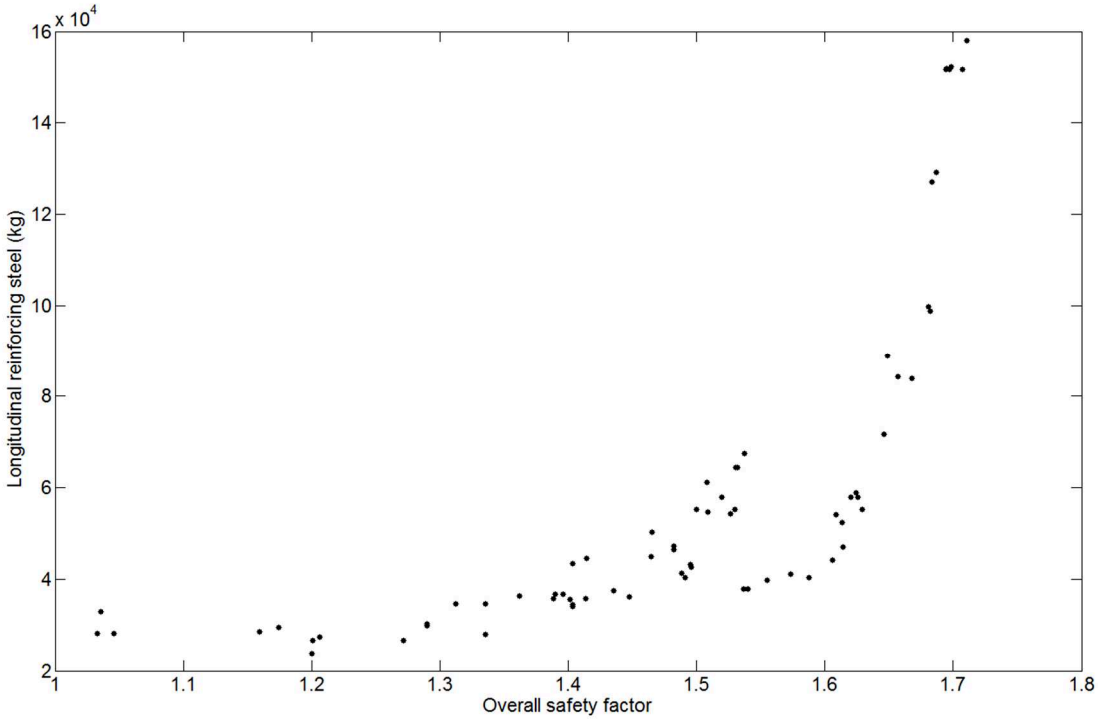

Fig. 13. Amount of longitudinal reinforcing steel according to overall safety factor.

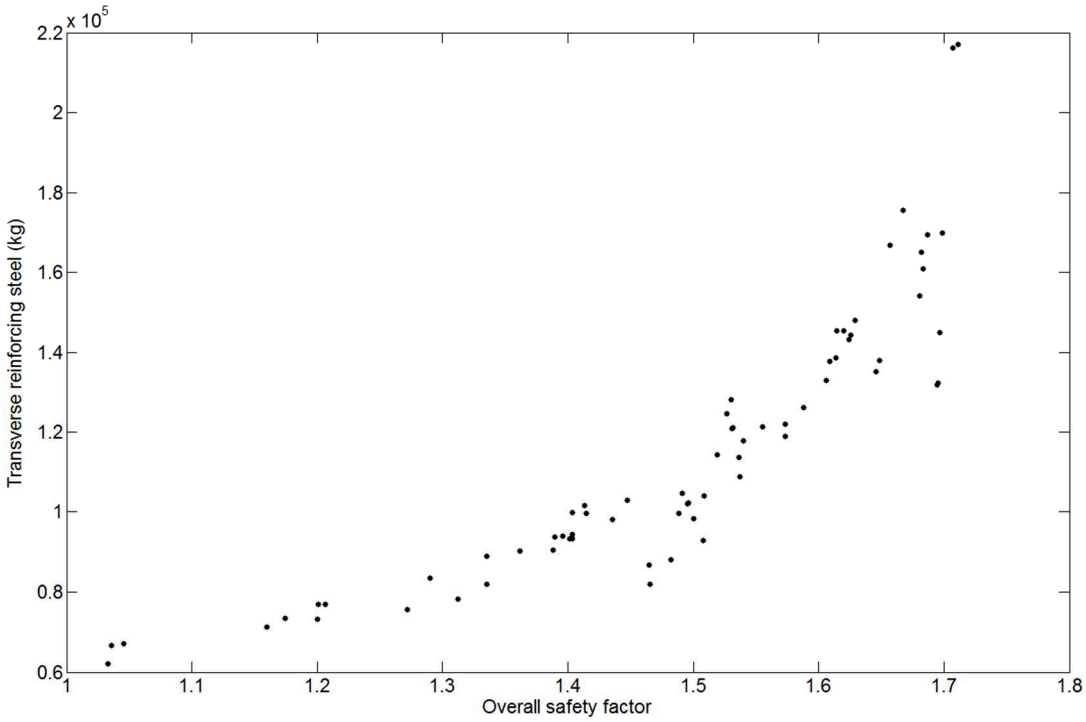

Fig. 14. Amount of transverse reinforcing steel according to overall safety factor.